tvst

Article

In Vitro Culture of Human Corneal Endothelium on Non-Mulberry Silk Fibroin Films for Tissue Regeneration

Charanya Ramachandran[1], Prerak Gupta[2], Swatilekha Hazra[1,4], and Biman B. Mandal[2,3]

[1] Prof. Brien Holden Eye Research Centre, LV Prasad Eye Institute, Hyderabad, Telangana, India
[2] Biomaterial and Tissue Engineering Laboratory, Department of Biosciences and Bioengineering, Indian Institute of Technology Guwahati, Guwahati, Assam, India
[3] Centre for Nanotechnology, Indian Institute of Technology Guwahati, Guwahati, Assam, India
[4] Manipal University, Manipal, India

Correspondence: Charanya Ramachandran, Prof. Brien Holden Eye Research Centre, LV Prasad Eye Institute, Hyderabad – 500034, Telangana, India. e-mail: charanya@lvpei.org, charanya.ram@gmail.com
Biman B. Mandal, Department of Biosciences and Bioengineering, Indian Institute of Technology Guwahati (IITG), Guwahati-781039, Assam, India. e-mail: biman.mandal@iitg.ac.in, mandal.biman@gmail.com

Received: October 24, 2019
Accepted: December 27, 2019
Published: March 9, 2020

Keywords: corneal endothelium; tissue engineering; biomaterial; non-mulberry silk

Citation: Ramachandran C, Gupta P, Hazra S, Mandal BB. In vitro culture of human corneal endothelium on non-mulberry silk fibroin films for tissue regeneration. Trans Vis Sci Tech. 2020;9(4):12, https://doi.org/10.1167/tvst.9.4.12

Purpose: The purpose of this study was to determine if non-mulberry varieties of silk are suitable for the culture of corneal endothelium (CE).

Methods: Aqueous silk fibroin derived from Philosamia ricini (PR), Antheraea assamensis (AA), and Bombyx mori (BM) were cast as approximately 15 µm films with and without pores on which human CE cells were cultured. Tensile strength, elasticity, transmittance in visible range, and degradation properties of the films were characterised. Adhesion of CE to the silk films was quantified using MTT assay in addition to quantifying the number and area of focal adhesions using paxillin. Expression of CE markers was determined at the gene and protein levels using PCR and immunostaining, respectively. Barrier integrity of the cultured cells was measured as permeability to FITC dextran (10 kDa) in the presence or absence of thrombin.

Results: The films exhibited robust tensile strength, >95% transmittance and a refractive index comparable to the native cornea. BM degraded significantly faster when compared to PR and AA. A comparison between the three varieties of silk showed that significantly more cells were adhered to PR and AA than to BM. This was also reflected in the expression of stable focal adhesions on PR and AA, thus enabling the formation of intact monolayers of cells on these varieties unlike on BM. Treatment with thrombin significantly increased cellular permeability to dextran.

Conclusions: Our data shows that PR and AA varieties sufficiently support the growth and function of CE cells. This could be attributed to the presence of natural cell binding motifs (RGD) in these varieties.

Translational Relevance: Development of a suitable carrier for engineering the CE to address a major clinical requirement of healthy donor tissues for transplantation.

Introduction

Diseases of the cornea resulting in either impaired vision or blindness are estimated to afflict over 35 million individuals globally with over 30,000 cases being added to the list every year.[1] The cornea is transparent and functions as the primary refracting element of the eye, hence, diseases afflicting it translate to thousands in man hours lost and, therefore, a huge loss to the economy. Replacing the affected cornea in part (lamellar or endothelial keratoplasty) or total (penetrating keratoplasty) with a healthy donor tissue is the current accepted standard of care. However, the huge gap in the demand and supply of healthy donor tissues is a well acknowledged bottleneck for timely

transplantations in many countries. Given that nearly a half of all the transplantations performed in a year are for replacing only the dysfunctional endothelium,[2] the monolayer of cells that maintain corneal transparency, research has focussed on engineering this layer in the laboratory.

Regeneration or replacement of these cells can be achieved by either directly injecting these cells into the anterior chamber[3] or delivering them as a monolayer using a carrier. The latter might be a better approach because the delivery would be precise, loss of transplanted cells would be lesser resulting in faster visual recovery, and the number of cells required for transplantation may be lesser. Thus, it is important to identify a substrate that closely mimics the native basement membrane of these cells, the Descemet' membrane, which is a transparent, elastic, thin (5–15 μm) structure composed primarily of collagen and matrix proteins, such as laminin and fibronectin. Several materials have been developed for this purpose, including decellularized corneal stroma, human amniotic membrane, collagen I sheet, silk fibroin, composite materials, hydrogel, gelatin, and synthetic materials.[4–11] However, each of these have limitations in terms of poor tensile strength, low transparency, poor compatibility, poor support for cell growth, or high cost.

Naturally derived silk protein is a potential biomaterial for various tissue engineering applications owing to its biocompatibility, tuneable degradability, remarkable mechanical strength, minimal immunogenicity, and ability to adopt myriad formats (3D scaffolds, nanofibers, hydrogels, thin films etc.).[12–15] Silk films prepared using the mulberry variety Bombyx mori (BM) are optically transparent, easy to handle, and has shown some promise for corneal regeneration by supporting the growth of corneal endothelial and epithelial cells.[11,16–22] However, to achieve confluent growth of these cells on BM, it is required to modify the silk films by Arg-Gly-Asp (RGD) coupling[23,24] or collagen coating.[11] This makes the fabrication process cumbersome and expensive, thus limiting the use of BM silk films for corneal tissue engineering purposes.[18] It is pertinent to note that most prior studies have used the BM silk for corneal regeneration applications whereas, various non-mulberry silk varieties remain largely unexplored. Some of these have been reported to possess cell-binding RGD motifs naturally,[25–27] thus rendering them more suitable for cell-based therapies. Hogerheyde et al. used a wild non-mulberry silk fibroin (NMSF) Antheraea pernyi for corneal epithelial cell transplantation.[28] In another study, Hazra et al. showed the potential of NMSF Antheraea mylitta as a superior alternative for growth of keratocytes and epithelial cells isolated from rat cornea when compared with BM silk.[29]

In this study, we report the use of silk protein, isolated from non-mulberry varieties Philosamia ricini (PR) and Antheraea assamensis (AA) for the culture of corneal endothelial cells and assess their ability to support human corneal endothelial growth and function in comparison to BM. We hypothesize that PR and AA would support cell adhesion and growth better than BM due to the natural presence of RGD motifs in these silk varieties.

Materials and Methods

Preparation of Silk Fibroin Solution

Aqueous silk fibroin (SF) protein was obtained from different sources viz. BM cocoon (mulberry variety), PR, and AA silk glands (non-mulberry variety) following previously reported protocols.[30–32] Briefly, BM cocoons were cut into small pieces and washed thoroughly in Milli-Q water. Sericin was removed by boiling the cocoon pieces in 0.02 M Na_2CO_3 for 30 minutes followed by fiber dissolution in 9.3 M lithium bromide (Sigma Aldrich, USA). The solution was dialyzed extensively in a 12 kDa molecular weight cut off dialysis membrane against Milli-Q water at room temperature (RT; 25 °C). AA and PR proteins were directly extracted from silk glands of matured fifth instar silkworm larvae. Extracted protein was further dissolved in 1% sodium dodecyl sulfate (SDS; Himedia, India) and dialyzed against Milli-Q water at 4°C for 4 hours. Percentage of aqueous protein solutions was calculated following the gravimetric method.

Fabrication of Silk Films

Silk films were fabricated by casting aqueous silk solution onto 4 cm × 4 cm polydimethylsiloxane (PDMS; Dow Corning Corporation, Midland, MI, USA) molds. The 2 mL of 2% (w/v) SF solution was cast upon PDMS molds and allowed to dry overnight in a laminar flow hood. Dried silk films were further subjected to water vapor annealing in a vacuum desiccator maintained at 30 mm Hg for 6 hours to induce water insolubility. Porous silk films were prepared by manually creating pores using 31 G needle (25 pores per 25 mm^2 area). Pores were created manually after experimenting with Poly-ethylene oxide (PEO), which proved to be toxic to the cells. Note: The non-porous silk films are referred to as "flat" films.

Morphological Assessment of Silk Films

Surface morphology of fabricated silk films was analyzed under Field emission scanning electron microscope (FESEM; Zeiss, Sigma) after gold sputtering. Silk films were subjected to FESEM analysis after dehydration using a series of graded ethanol. Images of porous silk films were captured using phase contrast microscopy (EVOS FL; Life Technologies, USA). Captured images were further processed using MBF ImageJ software (NIH, USA) to calculate the pore size on the porous silk film surface.

Fourier Transform Infrared Spectroscopy

Fourier transform infrared (FTIR) spectra of silk films (with and without water vapor annealing) was recorded in ATR mode using FTIR Spectrophotometer (Nicolet iS 10). Data was obtained in absorbance mode within 400 to 2000 cm^{-1} wavenumber range and 10 scans per spectra (4 cm^{-1} resolution).

Degradation Profile and Swelling Properties

Water vapor annealed flat silk films were analyzed for their degradation profile in the presence of 2 U/mL protease XIV (Sigma Aldrich, USA). The dry weight of 1 cm^2 silk films was recorded and they were immersed in enzyme solution prepared in phosphate buffered saline (PBS; pH 7.4) at 37°C. At predefined time points, the enzyme solution was removed and films were dried overnight in a dry hot air oven at 40°C. The dry weight of enzyme treated films was recorded. Degradation is reported in terms of % mass remaining at a particular time point calculated as follows:

$$\text{Mass remaining}\,(\%) = (\text{Dry weight at time t}) / (\text{Initial dry weight}) \times 100$$

Water retention capability of flat silk films (1 cm^2) was analysed in PBS at 37°C. Dry weight (W_d) of silk films was recorded prior to submerging them in PBS. At defined time points, wet weight (W_s) of swollen silk films was recorded after removing the excessive PBS. Swelling profile of silk films was calculated as follows:

$$\text{Swelling}\,(\%) = [(W_s - W_d)/W_d] \times 100$$

Mechanical Properties

Tensile properties of flat and porous silk films were analyzed using Universal Testing Machine (UTM; Instron, model 5944) equipped with 100 N load cell under ambient conditions.[32] Silk films were cut into 1 × 4 cm^2 rectangular strips and fitted in between the pneumatic grips keeping 3 cm working distance. Stress-strain curves were obtained in a dry condition at a crosshead rate of 1 mm/min following ASTMD 882−02 standard. Images of silk film cross sections were captured using the EVOS FL (Life Technologies) microscope and processed using Image J software to calculate the film thickness.Young's modulus of the films was calculated at 1% to 2% tensile strain whereas % elongation at break point was obtained by manually fitting the breakpoint values in the following formula:

$$\%\,\text{Elongation at break} = \frac{\text{Final Length (mm)} - \text{Initial Length (mm)}}{\text{Initial Length (mm)}} \times 100$$

All the data was recorded for $n = 10$ silk films.

Transparency

Flat silk fibroin films were scanned in the visible range (400−700 nm) with a step size of 5 nm. Absorbance was recorded using a multi-plate reader (Tecan infinite M 200 pro) and converted to percentage transmittance using Beer's law as follows:

$$A = 2 - \log_{10}\%T$$

where A = Absorbance and T = Transmittance.

Refractive Index

An imaging ellipsometer (Accurion) was used to calculate the refractive index of flat silk films at 658 nm incident wavelength aligned at 45° from the surface. The thickness of silk films was determined using microscopic cross-sections prior to data acquisition for refractive index. The data was recorded for three different points on silk films of each variety and reported as an average value.

Modulation Transfer Function

For analyzing the optical performance of the flat silk films, the two dimensional modulation transfer function (MTF) was measured using MATLAB software (Nantucket, MA, USA) using standard fourier optics technique. Images of the object were taken using a camera either in the presence or in the absence of wet silk films. The same image was optically blurred in order to be used as a control. The normalized power values were plotted as a function of the object frequency (cycles/picture). It is expected that in a natural scene, the optical performance will reduce with an increase in object spatial frequency. The

analysis determined if the MTF loss with silk film was any greater than or equal to the MTF loss without the films.

Culture of Human Corneal Endothelial Cells on Silk Films

Both primary cells (referred to as HCE-P) and the characterized cell line HCEnC-21T (referred to as HCE-21T) procured from Dr. Ula Jurkunas (Harvard Medical School, Boston, MA, USA) were used in subsequent experiments. Both the HCE-P[33,34] and the HCE-21T[35] cells were cultured based on prior publications. Donor corneas for culture were obtained from the Ramayamma International Eye Bank (LV Prasad Eye Institute, Hyderabad, India) following approval by the institutional review board. Both primary cells and the cell line were cultured in plastic dishes coated with fibronectin-collagen coating mix (FNC, Athena ES, USA). Primary cells between passages 1 and 3 were used in further experiments.

To culture cells, the silk films were cut into the required size and sterilized with 70% ethanol for 1 hour followed by a vigorous wash with 1X PBS. The films were conditioned with culture medium overnight at 37°C prior to seeding cells to assess for cell adhesion, growth, and function.

MTT Assay

The adhesion of corneal endothelium (CE) cells to the surface of silk films was quantified using the tetrazolium dye MTT as described earlier.[36] We punched out flat silk films of all the three varieties according to the size of 96-well plate, and post-sterilization, HCE cells were seeded on the films at a density of 200 cells/mm^2. The experiment was performed in triplicates, where plastic wells coated with FNC served as control. Two different experiments were performed: the same batch of silk was used with HCE-P cells from different donors ($n = 5$), to determine the biological variation in cell adhesion and in the other the HCE-21T cells were cultured on different batches ($n = 4$) of silk to determine the repeatability in the manufacturing of the silk films. The cells were allowed to attach for 30 minutes and the unattached cells were removed by gently washing the wells with culture medium. After 4 hours, 100 µl of 2.5 mg/mL of MTT salt (Invitrogen, Grand Island, NY, USA) was added to the cells and incubated for 1 hour. Following this, the MTT reagent was replaced with100 µl of dimethyl sulfoxide (Sigma Aldrich, USA). The absorbance value was measured at 540 nm using a spectrophotometer (SpectraMax M3, Molecular Devices, USA).

Quantification of Focal Adhesion

Focal adhesion (FA) in HCE-P cells on silk films was quantified using paxillin antibody (Invitrogen). Primary cells were cultured on flat silk films at a density of 200 cells/mm^2 for 2 different time points (30 minutes and 24 hours). Quantification was done at 30 minutes in order to corroborate with the MTT assay and at 24 hours to map any change in the distribution of the FAs once the cells were completely spread out. At each time point, the cells were fixed using 4% paraformaldehyde (Fisher Scientific, USA) and immunostained with paxillin followed by incubation in secondary antibody conjugated with alexafluor 488 (Invitrogen). Cells cultured on FNC coated glass coverslips were used as control. Images of 10 random cells were taken using a confocal microscope (Zeiss Airyspace LSM 880, Zeiss, Germany) at 63×. The size and area of the individual FA points and the total number of FA points per cell were quantified using Image J software following previously described protocol.[37]

Proliferation of HCE on Silk Films

The proliferation of HCE on flat silk films was determined using an antibody against Ki67 (Abcam, Cambridge, MA, USA), a specific marker for dividing cells. HCE-P cells were seeded on the films at 150 cells/mm^2 and cultured for 48 hours. The cells were fixed with 4% paraformaldehyde and immunostained for Ki67 using DAPI as counterstain. Images were captured in 10 different fields and a minimum of 500 cells were counted per film. The experiments were repeated twice. The percentage of dividing cells was quantified by using the following formula:

$$\%\,\text{proliferating cells} = \frac{\text{Cells expressing Ki}_{67}}{\text{Total number of cells}} \times 100$$

RNA Isolation and PCR

HCE-P cells were cultured on the three flat silk films for 2 weeks until they formed a mature monolayer. Total RNA was isolated from the cells using TRIZOL method. Nanodrop (Nanovue plus; GE Healthcare, USA) was used to quantify and assess the quality of RNA. The cDNA was synthesized using 1 µg of total RNA by using Superscript III cDNA synthesis kit (Invitrogen, USA). PCR was performed for endothelial markers as listed in Table 1. Glyceraldehyde 3-phosphate dehydrogenase (GAPDH) was used as an internal control. The PCR products were separated by agarose gel electrophoresis on 1.5% agarose gel, followed by detection under gel documen-

Table 1. Primer Sequence, Expected Band Size, and Annealing Temperature

Gene	Sense Primer	Anti-Sense Primer	Size (bp)	Annealing Temperature
ZO-1	**TTCTGAGGCCTGTAACCATTTT**	**AATTGGATACCACTGGGCATAG**	**245**	**58°**
Na/K ATPase	**ACGGCAGTGATCTAAAGGACAT**	**GAAGAATCATGTCAGCAGCTTG**	**255**	**60°**
VDAC3	**ATAAGTTGGCTGAAGGGTTGAA**	**TTCTGTGACAGTTTGGATTTGG**	**235**	**58°**
CLCN3	**GAGTTTTGCCTTTCTTGCAGTT**	**GAAAAGATATTTCCGCAGCAAC**	**203**	**58°**
p-120	**AGGATCCAGCAAACGATACAGT**	**AGGTCAGCTATGGCAGAAAGAG**	**244**	**56°**
GPC-4	**AGGTTGACACCAGCAAACCA**	**AAGAAGTCCACGTCGTTCCC**	**109**	**56°**
GAPDH	**GAGATCCCTCCAAAATCAAGTG**	**GAGTCCTTCCACGATACCAAAG**	**445**	**55°**

Table 2. Antibody Information

S. No	Antibody	Company	Species Raised in	Dilution Factor	Incubation Time
1	Phalloidin	Invitrogen	–	1:200	1 h room temp.
2	N-cadherin	Santa Cruz	Rabbit	1:50	16 hs at 4°C
3	ZO-1	Invitrogen	Rabbit	1:50	16 hs at 4°C
4	Na/K^+ ATPase	Santa Cruz	Mouse	1:50	16 hs at 4°C
5	Collagen 8	Sigma	Mouse	1:100	16 hs at 4°C
			Secondary Antibodies		
6	Alexa Fluor 488	Invitrogen	Goat (anti-Rabbit)	1:200	1 h room temp.
7	Alexa Fluor 488	Invitrogen	Goat (anti-Mouse)	1:200	1 h room temp.

tation system (Molecular imager Gel Doc XR+, Bio Rad, USA).

Immunofluorescence Staining

HCE-21T cells were seeded at a density of 1000 cells/mm^2 on the flat silk films and FNC coated coverslip (control). The cells were fixed using 4% paraformaldehyde for 10 minutes, then permeabilized using 0.1% Triton-X (Fisher Scientific, USA) and blocked using 2.5% bovine serum albumin (Sigma Aldrich, USA) for 1 hour at room temperature. CE markers, such as collagen 8 ZO-1, N-Cadherin, Na/K ATPase, and the cytoskeleton marker phalloidin were used to characterize the cells. Images were captured using Zeiss Airyspace LSM 880 confocal microscope. The details of the antibodies and the dilution factors are listed in Table 2.

Barrier Integrity of HCE Cells Cultured on Silk Films

In order to test the barrier integrity, HCE-P cells were grown to confluence on porous silk films obtained from PR and AA. BM was not used because the cells did not form an intact monolayer. The permeability was assessed using FITC-dextran (10 kDa; Sigma Aldrich, USA) as described earlier.[38] The experiments were performed in duplicates for each silk type and were repeated twice ($n = 3$). The cells were conditioned with serum-free medium for 1hr before treatment with or without thrombin (5U) for 1 hour. After removal of thrombin, FITC-dextran (0.5 µg/mL) was added for 2 hours and 100 µl of the sample from the basolateral chamber was removed for analysis. Fluorescence was measured at 518 nm using a spectrophotometer (SpectraMax M3; Molecular Devices, USA).

Statistical Analysis

All experiments were performed for at least $n = 3$ times unless otherwise specified and results are reported as mean ± SD. For significance analysis, 1-way ANOVA was performed following post hoc Tukey's test using Origin 8.0 software. Any P value < 0.05 was considered to be statistically significant.

Results

Surface Morphology of Silk Films

Silk films were visualized under FESEM to analyze the surface topography. PR and AA films showed

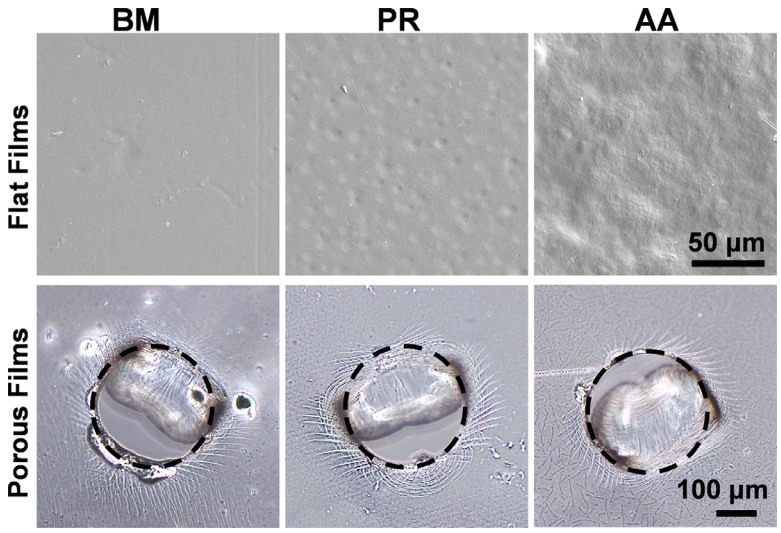

Figure 1. FESEM images of flat silk films showing the surface topography. Manually created pores in silk films were visualized under phase contrast microscope. Dotted black circles are representing single pore.

rougher surface as compared to BM silk films. This is in agreement with our previous reports.[32] To obtain porous silk films, we created pores by manual punching of 31 G needle into silk films. Consistency of pore distribution was maintained by creating 25 pores in each 5 × 5 mm^2 surface area. Pores created in this manner were of 290 ± 20 µm diameter and left behind a hemi circular flap (Fig. 1). The thickness of the silk films was 15 ± 2 µm and no significant difference was observed between the three varieties.

Fourier Transform Infrared Analysis

FTIR spectra of silk films were recorded to analyze the conformation and presence of secondary protein structures in silk films. All three films exhibited characteristic peptide backbone bands in amide I (1610−1660 cm^{-1}), amide II (1510−1560 cm^{-1}), and amide III (1210−1260 cm^{-1}) regions (Fig. 2A). Water vapor annealing led to a structural transition towards β-sheet structure (silk II) as confirmed by peak values 1610 to 1630 cm^{-1} (amide I) and 1510 to 1530 cm^{-1} (amide II) for treated samples from all three silk varieties.[39] Presence of β-sheet structural transition was further assured by assessing the water insolubility of silk films after water vapor annealing.

Degradation and Swelling Properties

The degradation profile of silk films is reported until 14 days in terms of percentage mass remaining at specific time points (Fig. 2B). The BM films degraded at a faster rate when compared to AA and PR films ($P < 0.05$). While approximately 65% of protein degradation was observed within 14 days of protease treatment for BM films, AA and PR films lost approximately 40% of their mass.

Swelling behavior of water vapor treated silk films was studied in PBS at 37°C. All three varieties of silk films swelled quickly within 30 minutes and attained a plateau within 2 hours (Fig. 2C). However, no significant difference was observed between swelling behaviors of different variety silk films ($P > 0.05$).

Mechanical Properties of Silk Films

Mechanical strength of a biomaterial is an important parameter to maintain the graft integrity under dynamic in vivo conditions after implantation. Tensile strength (Young's Modulus) and elasticity (% elongation at break) were calculated for all the silk film varieties in dry condition. AA films exhibited maximum tensile stress at break point followed by PR and BM films (Fig. 3A). Young's Modulus of BM and PR films were in the same range owing to almost similar slope of the stress-strain curve of these two variants. As quantified in Figure 3B, Young's Modulus of AA films was highest among different experimental groups and ranged between 1246 ± 36 MPa (almost 1.5 fold higher than the other two variants). The Young's modulus of porous films were comparable to the flat films indicating that the presence of pores did not alter the mechanical property of the films. On a similar note, the elasticity of various silk films was also determined manually and represented as % elongation at break (Fig. 3C). Non-mulberry films (PR and AA) extended more as compared to mulberry silk films, BM ($P < 0.01$). A approximately 1.4 fold higher elongation

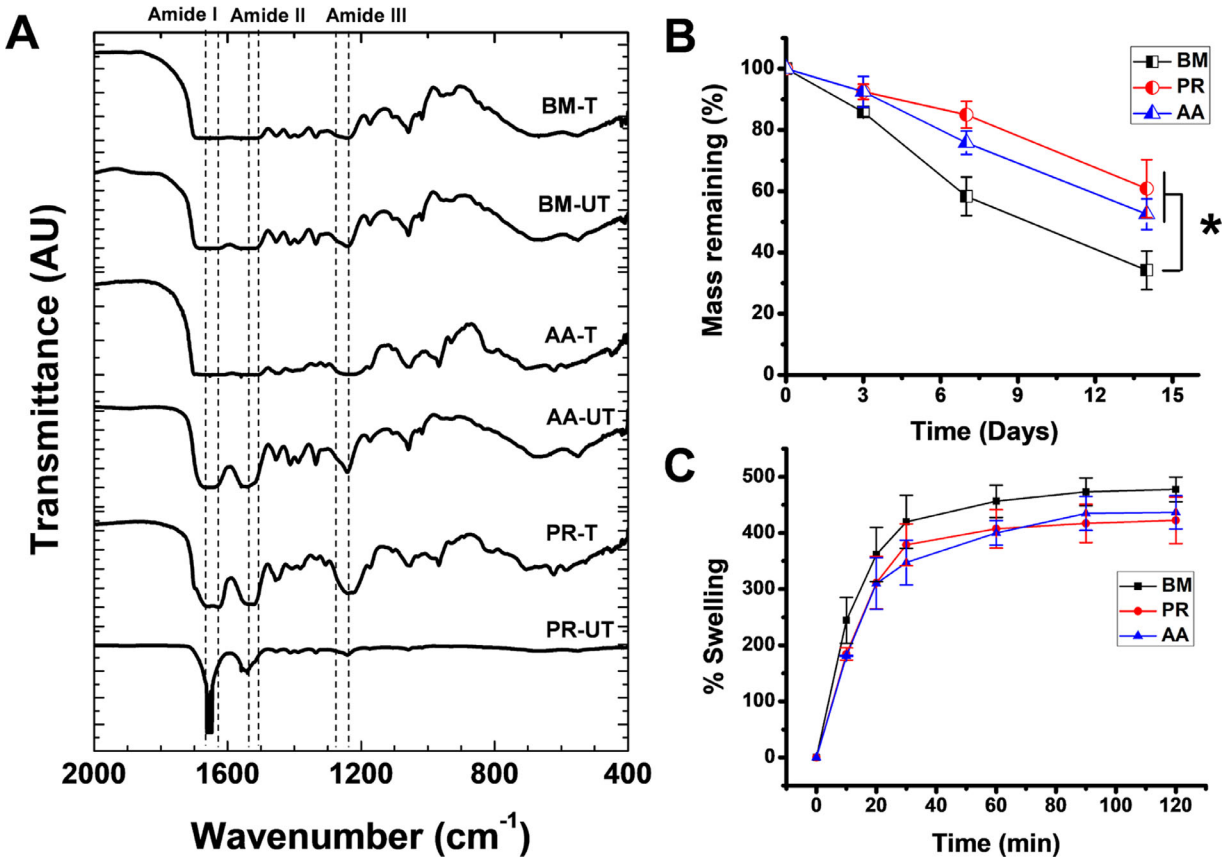

Figure 2. Physico-chemical characterization of flat silk films. (**A**) Fourier Transform Infrared (FTIR) spectra of water vapor treated (T) and untreated (UT) silk films. (**B**) Degradation profile of silk films in the presence of 2 units/mL of protease XIV in PBS (*$P < 0.05$). (**C**) Swelling profile of silk films over time at 37°C.

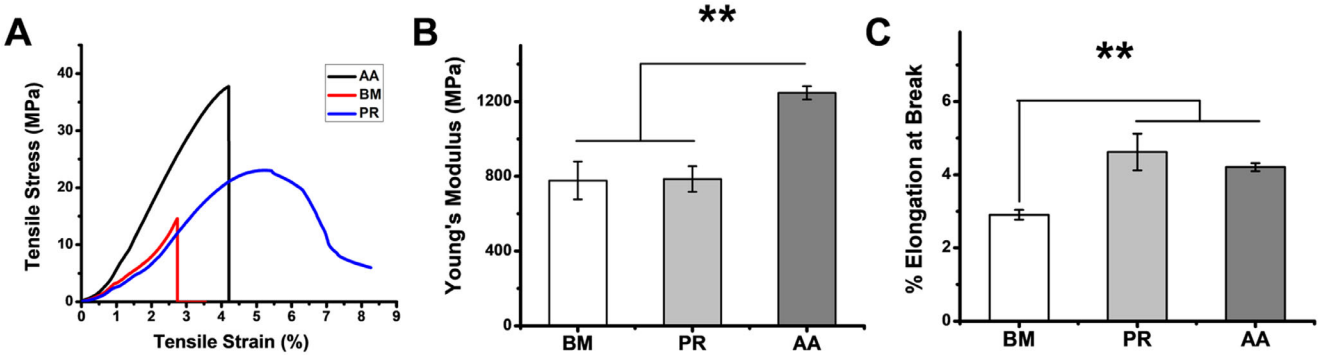

Figure 3. Mechanical properties of flat silk films. (**A**) Representative stress-strain curves, (**B**) Young's Modulus and (**C**) Percentage elongation calculated at break point (**$P < 0.01$).

(ranging between 3.5% and 4.5%) was observed for NMSFs as compared to BM films.

Transparency and Refractive Index of Silk Films

For silk to be used for endothelial regeneration, it needs to exhibit the optimum optical properties such that it aids in vision restoration. Transparency of the films was measured by recording the absorbance of silk films in the visible region (400 nm–700 nm). The gross visual appearance of silk films is depicted in Figure 4A. BM films were found to have light absorbance between 0.001 to 0.006 and 99.51 ± 0.44% transmittance. Similarly, NMSFs (PR and AA) exhibited light absorbance between 0.01 and 0.04. Percentage transmittance for PR and AA were 95.12 ± 1.78

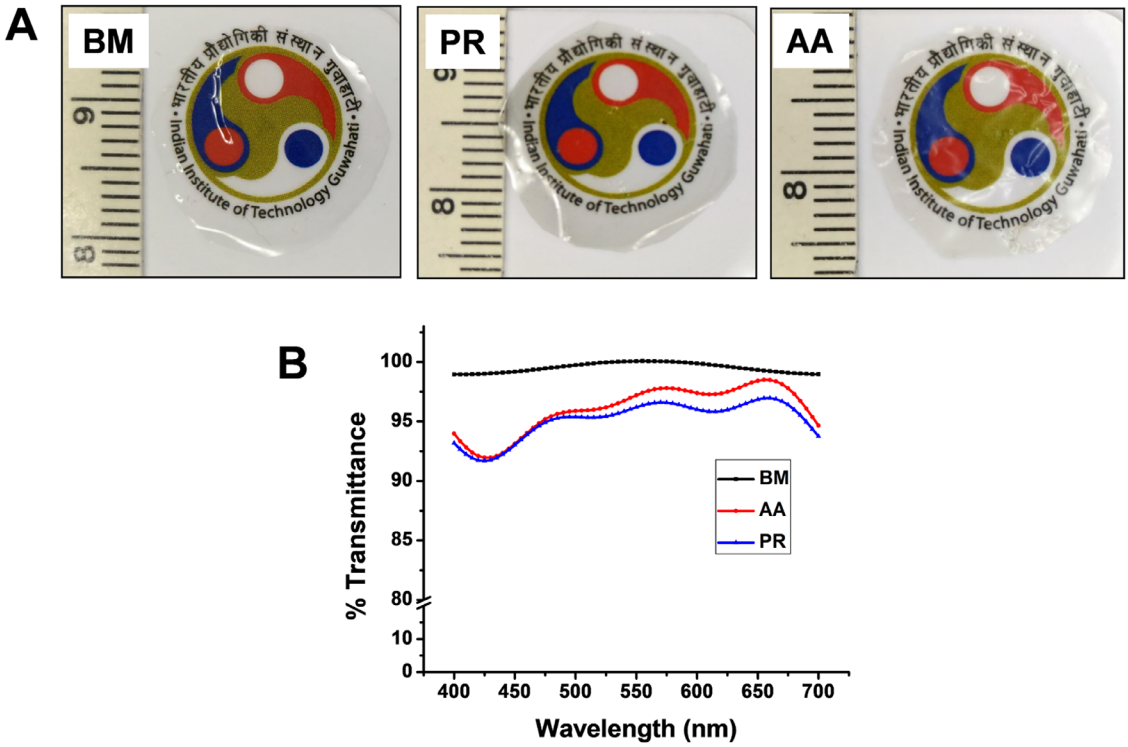

Figure 4. Transparency of silk films. (**A**) Representative images showing the visual appearance and transparency of silk films. (**B**) Spectra representing the percentage transmittance of silk films when scanned in the visible range (400–700 nm). All three silk film types were able to transmit >90% of the incident light.

and 96.02 ± 2.19, respectively (Fig. 4B). These values are in accordance with previous reports.[29]

We further confirmed the optical performance of the silk films by measuring their ability to transmit form information from the object to the image with high fidelity. This becomes an important feature to consider because the silk when wet (swollen) can reduce image quality despite being transparent. The MTF values were calculated for all the three films BM, PR, and AA. A focused high-resolution image of the object served as the positive control, whereas an optically blurred image served as the negative control (Fig. 5A). As expected, the performance of the films decreased at higher object spatial frequencies. However, this decrease was comparable to the positive control indicating that there was no degradation of information induced by the silk films. A faster drop off in the negative control indicates degraded optical quality induced by the blur leading to the poor transmittance of the information from the object at higher spatial frequencies (Fig. 5B).

Another crucial parameter to corroborate the suitability of silk films as a corneal implant is to assess their refractive index. For all three silk varieties, the refractive index was found to be approximately 1.49 (BM: 1.49 ± 0.005; AA: 1.49 ± 0.004; and PR: 1.49 ± 0.05). Interestingly, the refractive index values of silk films were close to human corneal epithelium (1.40).[40] Both transparency and refractive index values of silk films validate their potential to be used as a corneal implant.

Growth of HCE on Silk Films

At 2 hours after seeding, the cells could be seen adhered to all varieties of silk films (Figs. 6a–d). By 6 hours, the cells on PR and AA had started spreading similar to the cells on the plastic dish (Figs. 6e vs. 6g and 6h) however, the cells on BM were still rounded (Fig. 6f). Even after 24 hours, the cells on BM were in clumps (Fig. 6j) and not well spread out, unlike on PR and AA (Figs. 6k and 6l). The cells reached confluence within 5 to 7 days on PR and AA similar to on the plastic dish (Figs. 6o and 6p vs. 6m). Cells on BM slowly spread out over time but never reached confluence (Fig. 6n). Altering the density of cells seeded on the films (ranged from 250 cells/mm^2 to 3000 cells/mm^2) did not alter the growth pattern on these three films. At each seeding density, PR and AA films supported the formation of an intact monolayer. Moreover, cells cultured on PR and AA films were able to maintain the monolayer integrity for extended periods (3–4weeks,

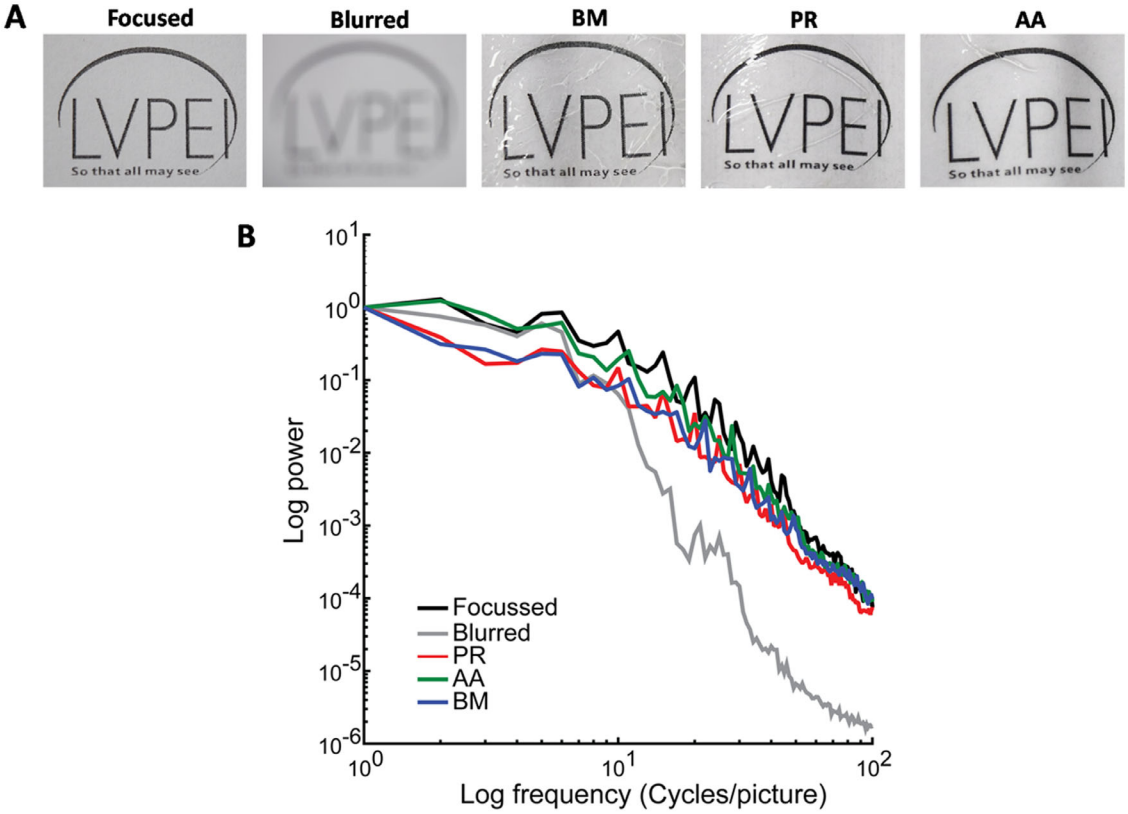

Figure 5. Optical performance of silk films. MTF graph representing the optical performance of the silk films BM, PR, and AA.There was degradation of information at higher spatial frequencies as expected, however, the presence of silk films did not increase the degradation.

the time required for the cells to mature functionally). On the contrary, cells cultured on the BM films either lifted off as sheets or clumped up when kept in long term culture (see inset in Fig. 6n).

Quantification of HCE Cell Adhesion and Proliferation on Silk Films

Because of the visible difference observed in the growth of HCE cells on PR and AA compared to BM, we quantified cell adhesion to the silk films (Fig. 7A). First, we cultured HCE-P from different donors on the films and found that significantly more cells were adhered to PR and AA when compared to BM ($P < 0.01$; Fig. 7B). There was no significant difference between PR and AA; however, the number of cells on the plastic plate was comparatively higher ($P < 0.01$). The cells adhered to the substrates in the following order of preference: plastic dish > PR ≥ AA > BM.

We further looked into the reproducibility of silk manufacturing process by testing different batches of silk using the HCE-21T cell line. Cell adhesion to the different silk films followed the same trend as primary cells (i.e., significantly higher cells were adhered to PR and AA compared to BM; Fig. 7C).

The strength of a cell's adhesion to its substrate is driven by the distribution of the FAs in the periphery, which, in turn, is regulated by the spreading of cells and force transmission from the substrate to the cell cytoskeleton. Thus, we quantified the average area of individual FA and number of FAs per cell in an attempt to better visualize the above noted difference in cell adhesion to the silk films. Cells were stained for paxillin at 30 minutes and 24 hours, as shown in Fig. 7D. After 30 minutes of adhesion, cells formed larger and more number of FAs on the FNC coated surface and PR compared to AA ($P < 0.001$; Fig. 7E and Table 7G). At 24 hours, the size of the FAs were significantly larger than on control ($P < 0.01$) and shown in Fig. 7F, but the average number of FAs were comparable between all three substrates. When compared between 30 minutes and 24 hours, there was a clear decrease in the number of FAs per cell concomitant with an increase in the average size of individual FAs. On BM, at 30 minutes, there were very few cells that had spread out, as shown in Fig. 7D, and individual FAs were not clearly visible in these cells for quantification. At 24 hours, some

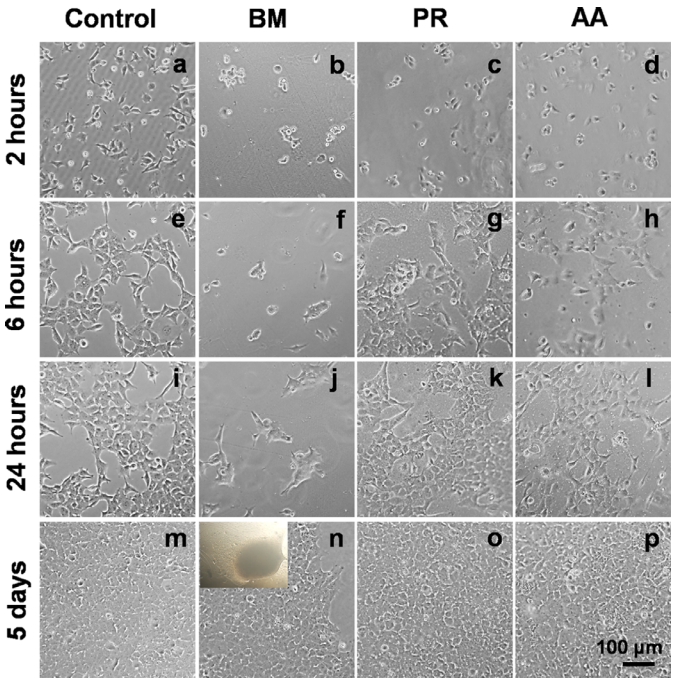

Figure 6. Phase contrast microscopic imaging of HCE-21T cells cultured on various silk films and on FNC coated tissue culture plate. Scale bar: 100 µm.

cells had spread in clumps but the individual FAs were still not clearly discernible for quantification (Fig. 7D). Because we could not quantify FAs reliably in BM, this was not included in the analysis.

In order to determine if the silk films supported cell proliferation, we used an antibody against Ki67, a cell proliferation marker, to quantify the same. The % proliferating cells in control was 85.75%, which was comparable to PR (75.69%) and AA (78.17%) but significantly higher compared to BM (69.74%; $P = 0.01$; Supplementary Fig. S1).

Characterization of HCE Cells Cultured on Silk Films

HCE cells were cultured on the silk films and characterized both at the gene and protein level using specific markers. Cells expressed endothelial specific genes, such as ZO-1, Na/K^+ATPase, voltage-dependent anion channel 3 (VDAC3), chloride channel protein 3 (CLCN3), glypican protein 4 (GPC-4), and p-120 catenin (Fig. 8A). HCE cells from fresh tissue served as the control for gene expression studies.

Unlike BM, staining with phalloidin showed that the cells on PR and AA exhibited a compact, uniform morphology, which was comparable to the control (Figs. 8B-a vs. 8B-c and 8B-d). Similarly, there was clear ZO-1, N-cadherin, and Na/K^+ ATPase expression at the cell boundaries in cells cultured on PR and AA similar to the control cells indicating that the cells are able to form a mature monolayer when cultured on these silk varieties. On BM, the expression of N-cadherin was at the membrane (Fig. 8B-f) but ZO-1 was mostly cytoplasmic (Fig. 8B-j) indicating that the cells formed a tight intercellular junction but were probably unable to mature into a functional monolayer. Cells on all silk varieties expressed collagen 8, a matrix protein unique to the CE, as seen in Fig. 8B (q-t). Because the cells on BM did not readily form a monolayer, we had to repeat staining several times and the best images are represented here.

Barrier Integrity of Cells Cultured on Silk Films

To quantify the functioning of the cells cultured on silk films, HCE-P were cultured until they formed a uniform and mature monolayer of cells and then treated with thrombin (5U). It is apparent from Figure 9 that there is a significant ($P < 0.001$) increase in cell permeability to dextran indicating that the cells cultured on the PR and AA silk films were able to form a compact monolayer of cells with tight intercellular junctions as would be expected.

Discussion

Any material being developed for tissue engineering purposes needs to be compatible, affordable, degradable, and allow resident cells to grow and function as required. In specific, any material to be used in the pupillary axis of the eye has to be transparent and exhibit optimum optical performance in order to enable good visual outcome.

Fibroin derived from different varieties of silk has been used extensively in tissue engineering applications[16] and in the eye the BM variety has been used to culture CE cells and for constructing the stroma.[41] The BM silk has also been used for the culture of HCE cells but with limited success in the absence of additional surface modifications, such as with collagen 1 or RGD peptides, which is in agreement with our present data. In contrast, cell adhesion to PR and AA was comparable to that of the FNC coated plastic dish even in the absence of surface modifications, as quantified using the MTT assay. We then took a closer look at the FAs because these are the primary sites of cell adhesion to the substrate in an attempt to better visualize the above noted difference. The FAs are complex multimolecular assemblies with several types of proteins that link the extracellular matrix, via membrane-bound receptors,

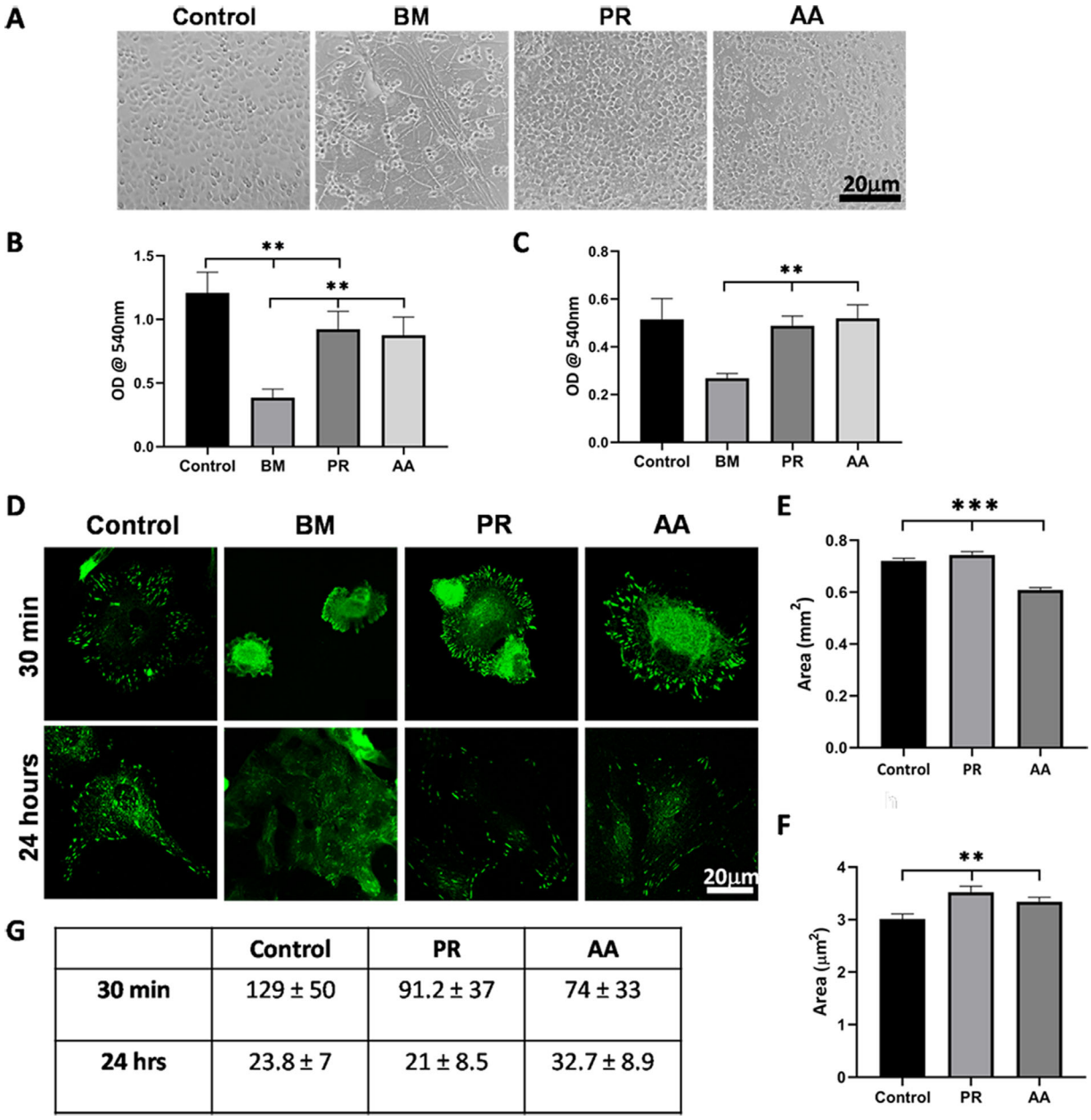

G

	Control	PR	AA
30 min	129 ± 50	91.2 ± 37	74 ± 33
24 hrs	23.8 ± 7	21 ± 8.5	32.7 ± 8.9

Figure 7. Quantificationof CE cell adhesion to silk films. (**A**) Representative images of cells adhered to the different silk films and FNC coated dish after 30 minutes. (**B**) Graph representing the adhesion of primary CE cells to the different varieties of silk films from the same batch. (**C**) Graph representing the adhesion of HCE-21T cell line to different batches of silk films. (**D**) Representative images of cells stained for paxillin at 30 minutes and 24 hours after seeding. (**E**) Graph showing the average area of FAs after 30 minutes of seeding and (**F**) at 24 hours after seeding. (**G**) Table of the average number of FAs at 30 minutes and 24 hours of seeding cells (**$P < 0.01$; ***$P < 0.001$).

to the cell's cytoskeleton.[42] Their size, numbers, total area occupied in a cell, and their distribution within the cells are all factors known to regulate cell adhesion strength and influence several cellular functions. At 30 minutes, discrete FAs (<1 µm) were visible in cells on control, PR, and AA but not on BM indicating that these cells were unable to even form nascent adhesions at this time point. This finding corroborates well with the result of the adhesion assay, which showed that fewer cells were able to adhere to BM at 30 minutes. The subsequent increase in the average size of FAs at 24 hours with a concomitant decrease in the number of FAs per cell is likely due to the aggregation of the nascent adhesions to form stronger and more stable attachments to the substrate. On BM, at the same time point, FAs were appreciable but appeared much smaller, clustered, and more like nascent adhesions. Better adhesion of cells to AA and PR meant that

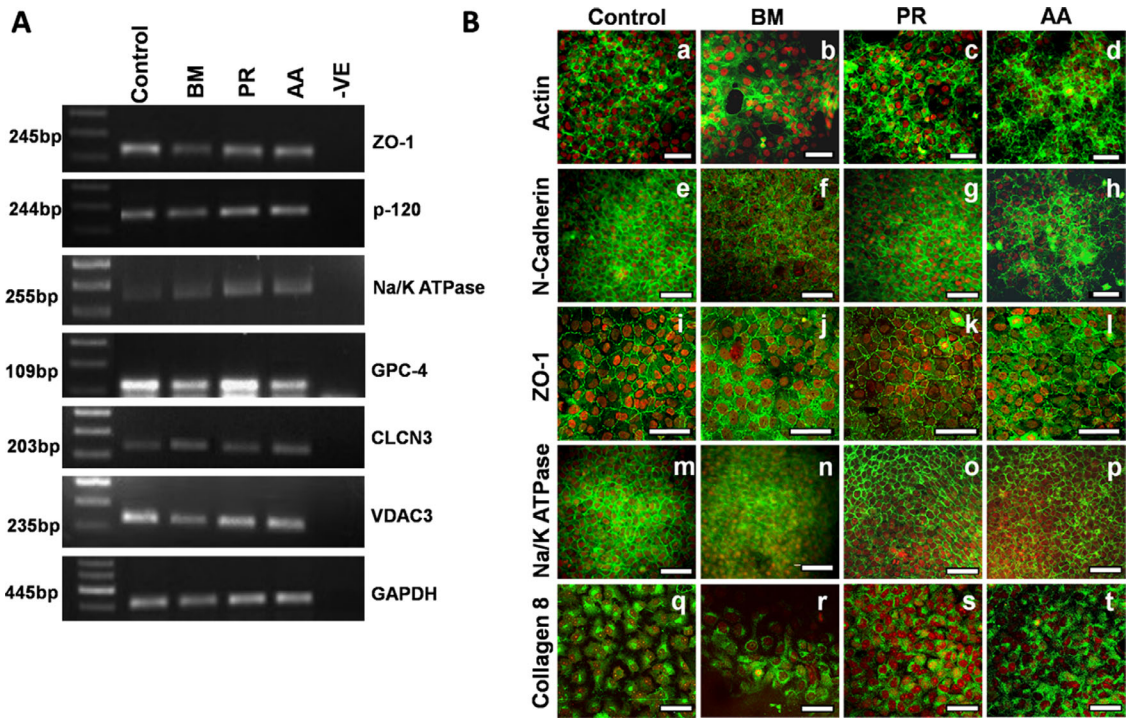

Figure 8. Characterization of HCE cells on silk. (**A**) Expression of genes specific to the CE and involved in the functioning of these cells. RNA isolated from fresh tissue was used as control. (**B**) Cells cultured on the silk films showing compact polygonal morphology seen as the peri-junctional actin ring due to staining with phalloidin. The cells also expressed markers for endothelial cells such as N-cadherin, ZO-1, Na/K ATPase, and Collagen 8. Note: Green: represents endothelial markers as mentioned in each row, Red: propidium iodide (PI); nuclear marker, magnification: 40 × (Scale bar: 50 µm). Images of ZO-1 have been optically zoomed by 1.5 × in order to visualize the staining better.

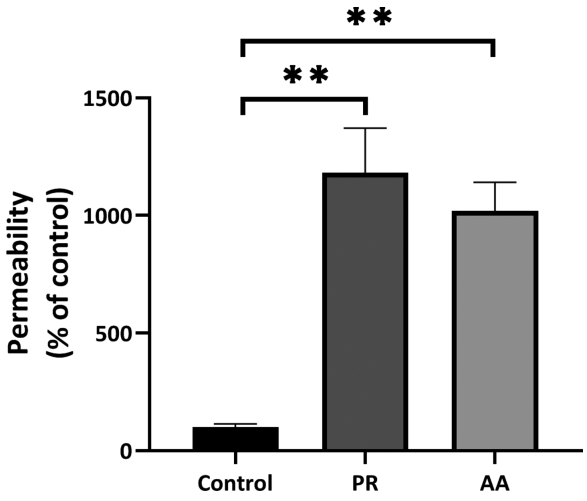

Figure 9. Permeability of HCE cells to FITC-dextran. The graph shows the significant increase in the permeability of HCE cells to dextran when the intercellular barrier was disrupted using thrombin (**$P < 0.01$).

the cells formed a compact, homogeneous monolayer of cells unlike on BM wherein the cells just clumped up or lifted off as sheets confirming that their intercellular adhesion was stronger than their adhesion to the silk. This differential support by the silk films for cell adhesion could likely be attributed to the presence of the repetitive RGD peptide sequence in the protein structure of PR and AA, which is known to be lacking in BM silk.[43,44]

Further phenotypic characterization confirmed that the cells expressed all the markers of the CE both at the gene as well as at the protein levels. An obvious difference was noted in the location of the tight junction protein ZO-1, which was mostly cytosolic in BM unlike in PR and AA indicating that the cells had not matured into a functional monolayer. The tight junctions in the HCE are required to establish intercellular barrier and cell polarity thereby enabling pump function.[45] We directly measured the barrier integrity of the cells by quantifying their permeability to FITC-dextran, which increased only in the presence of thrombin, an agent known to disrupt the barrier integrity of these cells by increasing the contraction of the cortical actomyosin complex. This in corroboration with the immunostaining data confirms that the silk films PR and AA are able to support HCE growth and function satisfactorily.

For silk to be used for endothelial regeneration, it needs to exhibit the optimum mechanical and optical properties. Good tensile strength and elastic properties

of the silk films are crucial parameters for dictating structural integrity. In agreement with previous reports, non-mulberry silk varieties were more elastic that BM silk owing to the presence of poly-alanine stretches without any intervening amino acids.[44] Although the tensile strength of the three silk films are much greater than the native substrate of the HCE (Descemet's membrane), they (PR and AA) were able to sufficiently support the growth and function of the cells without altering their phenotype.

The clinical advantage of the robust mechanical strength of the silk films would be the ease of handling the thin films a problem often faced with the commonly used collagen based materials. This would allow the surgeon to perform a Descemet's membrane endothelial keratoplasty (DMEK) surgery instead of the Descemet's stripping endothelial keratoplasty (DSEK) surgery, helping overcome the most important problem of haze formation due to misalignment of stromal collagen fibers. At present, preparing the DMEK lenticule or performing surgeries with it requires a lot of skill and training primarily because the lenticule folds inward making it difficult to manipulate it within the eye. The silk fibroin films by virtue of their tensile strength maintain their shape, thus making it easier to handle them. In addition, the thin films, which are of the same thickness as the adult native Descemet's membrane, are very flexible and it is, therefore, expected that the films will conform to the shape of the cornea when grafted.

Rate of biomaterial degradation is another crucial aspect that determines graft success. The implanted material should be tuned in such a way that its rate of degradation matches the rate of neo tissue formation. Non-specific enzyme activity would allow maximum degradation and would mimic the in vivo conditions where a cocktail of protein degrading enzymes is present in the vicinity of the implant. The degradation pattern of silk films suggested comparatively faster mass loss for BM films than AA and PR films. Such degradation behavior might be attributed to native amino acid composition of different silk varieties. Non-mulberry silk varieties possess higher content of hydrophobic residues leading to comparatively closed packing prohibiting access to the external aqueous microenvironment and minimal degradation.[32] The slower degradation might be advantageous because it is known that the secretion of basement material by HCE cells in vivo is very slow. However, the actual degradation of the material will be best studied in an animal model. Finally, we assessed the water retention capacity (swelling) of the films, which is imperative for cell viability because it allows the retention of nutrients and cell growth media. Over the course of 120 minutes, we did not observe any significant difference among the 3 silk varieties; however, BM silk retained slightly higher content of water when compared with its counterparts. It may again be related to the higher hydrophilic amino acid content of BM silk.

All of these aforementioned properties of silk films are important for any tissue engineering application; however, their implementation for corneal regeneration requires optical transparency. We quantified the same in terms of light absorbance, percentage transmittance, and refractive index in accordance with a previous study.[46] All of the silk films showed >90% transmittance of light and good optical performance. Moreover, the refractive index of silk films is very close to human cornea further substantiating their suitability for corneal regeneration.[40]

Finally, it is important that the material produced is cost effective, easy to source, and amenable to bulk manufacturing. The PR and AA films produced for this study were derived from the glands of the silk worm and we were able to extract 0.25 gm of fibroin protein from one gland. This can be used to fabricate 64 corneal discs of 1.2 cm, thus making these films affordable and favorable to bulk production.

Conclusions

This study demonstrates the development, characterization, and in vitro evaluation of different varieties of silk as a substrate for the culture of the corneal endothelium. The study shows that optically transparent membranes with good tensile strength, degradability, and refractive index matching the rest of the cornea can be produced reliably. Importantly, we have demonstrated the suitability of using fibroin from the non-mulberry varieties of silk (PR and AA), without additional structural or surface modifications, for culturing corneal endothelial cells. These silk varieties were able to better support the adhesion, growth, and function of the CE cells when compared to the more commonly used BM.

Acknowledgments

The authors thank Central Instruments Facility (CIF), IIT Guwahati, for providing high-end instruments.

This work was supported by the Department of Biotechnology grant BT/PR11885/MED/31/272/2014 (CR and BBM). The funding source did not participate

in the conceptualization, conduct or reporting of this study.

Disclosure: **C. Ramachandran,** None; **P. Gupta,** None; **S. Hazra,** None; **B.B. Mandal,** None

References

1. Gupta N, Tandon R, Gupta SK, Sreenivas V, Vashist P. Burden of corneal blindness in India. *Indian J Community Med*. 2013;38:198–206.
2. Tan DT, Dart JK, Holland EJ, Kinoshita S. Corneal transplantation. *Lancet*. 2012;379:1749–1761.
3. Kinoshita S, Koizumi N, Ueno M, et al. Injection of cultured cells with a ROCK inhibitor for bullous keratopathy. *N Engl J Med*. 2018;378:995–1003.
4. Lange TM, Wood TO, McLaughlin BJ. Corneal endothelial cell transplantation using Descemet's membrane as a carrier. *J Cataract Refract Surg*. 1993;19:232–235.
5. Hsiue GH, Lai JY, Chen KH, Hsu WM. A novel strategy for corneal endothelial reconstruction with a bioengineered cell sheet. *Transplantation*. 2006;81:473–476.
6. Ishino Y, Sano Y, Nakamura T, et al. Amniotic membrane as a carrier for cultivated human corneal endothelial cell transplantation. *Invest Ophthalmol Vis Sci*. 2004;45:800–806.
7. Mimura T, Yamagami S, Yokoo S, et al. Cultured human corneal endothelial cell transplantation with a collagen sheet in a rabbit model. *Invest Ophthalmol Vis Sci*. 2004;45:2992–2997.
8. Wang TJ, Wang IJ, Chen S, Chen YH, Young TH. The phenotypic response of bovine corneal endothelial cells on chitosan/polycaprolactone blends. *Colloids Surf B Biointerfaces*. 2012;90:236–243.
9. Hadlock T, Singh S, Vacanti JP, McLaughlin BJ. Ocular cell monolayers cultured on biodegradable substrates. *Tissue Eng*. 1999;5:187–196.
10. Mohay J, Lange TM, Soltau JB, Wood TO, McLaughlin BJ. Transplantation of corneal endothelial cells using a cell carrier device. *Cornea*. 1994;13:173–182.
11. Madden PW, Lai JN, George KA, Giovenco T, Harkin DG, Chirila TV. Human corneal endothelial cell growth on a silk fibroin membrane. *Biomaterials*. 2011;32:4076–4084.
12. Gupta P, Adhikary M, M JC, Kumar M, Bhardwaj N, Mandal BB. Biomimetic, osteoconductive non-mulberry silk fiber reinforced tricomposite scaffolds for bone tissue engineering. *ACS Appl Mater Interfaces*. 2016;8:30797–30810.
13. Mandal BB, Grinberg A, Gil ES, Panilaitis B, Kaplan DL. High-strength silk protein scaffolds for bone repair. *Proc Natl Acad Sci USA*. 2012;109:7699–7704.
14. Kumar M, Gupta P, Bhattacharjee S, Nandi SK, Mandal BB. Immunomodulatory injectable silk hydrogels maintaining functional islets and promoting anti-inflammatory M2 macrophage polarization. *Biomaterials*. 2018;187:1–17.
15. Bhunia BK, Kaplan DL, Mandal BB. Silk-based multilayered angle-ply annulus fibrosus construct to recapitulate form and function of the intervertebral disc. *Proc Natl Acad Sci USA*. 2018;115:477–482.
16. Lawrence BD, Marchant JK, Pindrus MA, Omenetto FG, Kaplan DL. Silk film biomaterials for cornea tissue engineering. *Biomaterials*. 2009;30:1299–1308.
17. Bray LJ, George KA, Ainscough SL, Hutmacher DW, Chirila TV, Harkin DG. Human corneal epithelial equivalents constructed on Bombyx mori silk fibroin membranes. *Biomaterials*. 2011;32:5086–5091.
18. Bray LJ, George KA, Hutmacher DW, Chirila TV, Harkin DG. A dual-layer silk fibroin scaffold for reconstructing the human corneal limbus. *Biomaterials*. 2012;33:3529–3538.
19. Vazquez N, Rodriguez-Barrientos CA, Aznar-Cervantes SD, et al. Silk fibroin films for corneal endothelial regeneration: Transplant in a rabbit descemet membrane endothelial keratoplasty. *Invest Ophthalmol Vis Sci*. 2017;58:3357–3365.
20. Liu J, Lawrence BD, Liu A, Schwab IR, Oliveira LA, Rosenblatt MI. Silk fibroin as a biomaterial substrate for corneal epithelial cell sheet generation. *Invest Ophthalmol Vis Sci*. 2012;53:4130–4138.
21. Abdel-Naby W, Cole B, Liu A, et al. Silk-derived protein enhances corneal epithelial migration, adhesion, and proliferation. *Invest Ophthalmol Vis Sci*. 2017;58:1425–1433.
22. Gosselin EA, Torregrosa T, Ghezzi CE, et al. Multi-layered silk film coculture system for human corneal epithelial and stromal stem cells. *J Tissue Eng Regen Med*. 2018;12:285–295.
23. Gil ES, Mandal BB, Park SH, Marchant JK, Omenetto FG, Kaplan DL. Helicoidal multilamellar features of RGD-functionalized silk biomaterials for corneal tissue engineering. *Biomaterials*. 2010;31:8953–8963.
24. Wu J, Rnjak-Kovacina J, Du Y, Funderburgh ML, Kaplan DL, Funderburgh JL. Corneal

stromal bioequivalents secreted on patterned silk substrates. *Biomaterials*. 2014;35:3744–3755.
25. Gupta AK, Mita K, Arunkumar KP, Nagaraju J. Molecular architecture of silk fibroin of Indian golden silkmoth, Antheraea assama. *Sci Rep*. 2015;5:12706.
26. Datta A, Ghosh AK, Kundu SC. Differential expression of the fibroin gene in developmental stages of silkworm, Antheraea mylitta (Saturniidae). *Comp Biochem Physiol B Biochem Mol Biol*. 2001;129:197–204.
27. Arunkumar KP, Tomar A, Daimon T, Shimada T, Nagaraju J. WildSilkbase: An EST database of wild silkmoths. *BMC Genomics*. 2008;9:338.
28. Hogerheyde TA, Suzuki S, Stephenson SA, et al. Assessment of freestanding membranes prepared from Antheraea pernyi silk fibroin as a potential vehicle for corneal epithelial cell transplantation. *Biomed Mater*. 2014;9:025016.
29. Hazra S, Nandi S, Naskar D, et al. Non-mulberry silk fibroin biomaterial for corneal regeneration. *Sci Rep*. 2016;6:21840.
30. Rockwood DN, Preda RC, Yucel T, Wang X, Lovett ML, Kaplan DL. Materials fabrication from Bombyx mori silk fibroin. *Nat Protocols*. 2011;6:1612–1631.
31. Mandal BB, Kundu S. A novel method for dissolution and stabilization of non-mulberry silk gland protein fibroin using anionic surfactant sodium dodecyl sulfate. *Biotechnol Bioeng*. 2008;99:1482–1489.
32. Gupta P, Kumar M, Bhardwaj N, et al. Mimicking form and function of native small diameter vascular conduits using mulberry and non-mulberry patterned silk films. *ACS Appl Mater Interfaces*. 2016;8:15874–15888.
33. Chen KH, Azar D, Joyce NC. Transplantation of adult human corneal endothelium ex vivo: A morphologic study. *Cornea*. 2001;20:731–737.
34. Zhu C, Joyce NC. Proliferative response of corneal endothelial cells from young and older donors. *Invest Ophthalmol Vis Sci*. 2004;45:1743–1751.
35. Schmedt T, Chen Y, Nguyen TT, Li S, Bonanno JA, Jurkunas UV. Telomerase immortalization of human corneal endothelial cells yields functional hexagonal monolayers. *PLoS One*. 2012;7:e51427.
36. Miki I, Ishihara N, Otoshi M, Kase H. Simple colorimetric cell-cell adhesion assay using MTT-stained leukemia cells. *J Immunol Methods*. 1993;164:255–261.
37. Horzum U, Ozdil B, Pesen-Okvur D. Step-by-step quantitative analysis of focal adhesions. *MethodsX*. 2014;1:56–59.
38. Shivanna M, Rajashekhar G, Srinivas SP. Barrier dysfunction of the corneal endothelium in response to TNF-alpha: Role of p38 MAP kinase. *Invest Ophthalmol Vis Sci*. 2010;51:1575–1582.
39. Lu Q, Hu X, Wang X, et al. Water-insoluble silk films with silk I structure. *Acta Biomaterialia*. 2010;6:1380–1387.
40. Patel S, Marshall J, Fitzke FW. Refractive index of the human corneal epithelium and stroma. *J Refract Surg*. 1995;11:100–141.
41. Chirila T, Barnard Z, Zainuddin Harkin DG, Schwab IR, Hirst L. Bombyx mori silk fibroin membranes as potential substrata for epithelial constructs used in the management of ocular surface disorders. *Tissue Eng Part A*. 2008;14:1203–1211.
42. Yamada KM, Geiger B. Molecular interactions in cell adhesion complexes. *Curr Opin Cell Biol*. 1997;9:76–85.
43. Ahmad R, Kamra A, Hasnain SE. Fibroin silk proteins from the nonmulberry silkworm Philosamia ricini are biochemically and immunochemically distinct from those of the mulberry silkworm Bombyx mori. *DNA Cell Biol*. 2004;23:149–154.
44. Gupta A, Mita K, Arunkumar KP, Nagaraju J. Molecular architecture of silk fibroin of Indian golden silkmoth, Antheraea assama. *Sci Rep*. 2015;5:12706.
45. Srinivas SP. Dynamic regulation of barrier integrity of the corneal endothelium. *Optom Vis Sci*. 2010;87:E239–254.
46. Hazra S, Nandi S, Naskar D, et al. Non-mulberry silk fibroin biomaterial for corneal regeneration. *Sci Rep*. 2016;6:21840.